07

Memristors for non-volatile resistive memory based on an $Al_2O_3/ZrO_2(Y)$ dielectric bilayer

© A.V. Kruglov, D.A. Serov, A.I. Belov, M.N. Koryazhkina, I.N. Antonov, S.Yu. Zubkov, R.N. Kriukov, A.N. Mikhaylov, D.O. Filatov, O.N. Gorshkov

Lobachevsky University of Nizhny Novgorod,
603022 Nizhny Novgorod, Russia
e-mail: krualex@yandex.ru

Received June 13, 2024
Revised August 1, 2024
Accepted September 25, 2024

In the present paper, memristors based on an $Al_2O_3/ZrO_2(Y)$ dielectric bilayer with an Al_2O_3 layer of 0, 3, 6 and 9 nm in thickness fabricated by magnetron sputtering, were investigated. The presence of the additional Al_2O_3 layer between the chemically active Ta electrode and the $ZrO_2(Y)$ functional dielectric allows localizing the sites of rupture and subsequent restore of the filaments during cyclic resistive switching and leads to an improvement in the stability of the resistive states of the memristor. The as fabricated memristor stacks with different thicknesses of the Al_2O_3 can be either in the conductive state or in the non-conductive one. The stacks being in different resistive states initially and subjected to electroforming or „antiforming"did not demonstrate significant differences in the values of switching currents and voltages during subsequent measurements. The results obtained can be applied in the development of the „forming-free" memristors, which are relevant for their CMOS integration.

Keywords: memristor, resistive memory, resistive switching, filament, current-voltage curves, electroforming, yttria-stabilized zirconia, alumina.

DOI: 10.61011/TP.2024.11.59748.204-24

Introduction

Memristors are key elements of the new component base of micro- and nanoelectronics and the basis for both digital devices of Resistive Random Access Memory [1] and analog devices used for hardware implementation of neuromorphic information and computing systems based on the principles of brain functioning [2]. The development of reliable (with reproducible and stable characteristics) memristors is one of the most urgent scientific and technical tasks that need to be reached for creating the above-mentioned devices and computing systems.

It is necessary to ensure compatibility of the materials used and the operating parameters of memristor devices with the parameters of control elements and CMOS circuits for successful integration of memristors into the manufacturing process of complementary structures metal–oxide–semiconductor (CMOS). In addition, they should ensure a large number of resistive switching (RS), low dispersion and stability of resistive states over time, as well as low power consumption.

One of the most serious problems of memristor electronics, which limits widespread practical implementation, is the low reproducibility from cycle to cycle and from device to device of the key parameters of RS memristors [3], such as RS voltages and current values through the device in a state with high (HRS, high resistance state) and low (LRS, low resistance state) resistance, as well as their degradation during operation. The variation of RS parameters has a fundamental origin, namely, it is associated with the stochastic nature of the processes underlying it [4].

The need to reduce the voltage of electroforming is an important task for the practical use of memristor devices, especially in conjunction with low-power CMOS devices [5] when a soft (reversible) breakdown of a functional dielectric occurs, and ideally the creation of memristor devices that demonstrate RS without electroforming [6,7].

The so-called filamentous RS mechanism is implemented in most of the developed memristor designs to date, which consists in the restoration and destruction of conductive cords (filaments) under the action of an electric field between the electrodes of the memristor structure. Filaments are formed, as a rule, from oxygen vacancies in metal oxide-based memristors [8]. Usually, the memristor is switched from the LRS to the HRS (RESET process) and back (SET process) by rearranging the vacancy structure of the filament near the boundary with one of the electrodes (at a distance of about several nanometers). At the same time, the diameter of the filament can also be several nanometers. Thus, the switching processes occur in a small volume of material (on the order of several cubic nanometers) regardless of the size of the memristor itself near the interface of the filament with one of the electrodes, and a small (countable) number of ions (oxygen vacancies) is involved in the switching process. In this case, each ion jump to an adjacent vacancy changes the structure of the filament (and, consequently, its conductivity). The main way to improve the characteristics of memristors is based on a materials science approach and consists in choosing

the optimal materials and manufacturing technology for memristor structures.

The papers [4,5,9–15] showed earlier that the use of two-layer (multilayer) structures as a functional dielectric is one of the ways to stabilize the RS parameters and improve the characteristics of memristors. A significant number of studies have been carried out to date in which aluminum oxide Al_2O_3 (or AlO_x) was used as an additional insulating layer material, and HfO_2 was used as a functional dielectric [16–25]. Special attention was paid to the role of the thickness of the additional layer and its position in memristor structures obtained by atomic layer deposition. In particular, the paper [24] demonstrated the effect of the thickness of layer of Al_2O_3 (0, 5 and 10 nm) on the stability of RS parameters in $TiN/Al_2O_3/HfO_2/Pt$ structures. A decrease of switching voltages V_{SET} and V_{RESET} and their spread is observed, as well as stabilization of the resistance values R_{HRS} and R_{LRS} in the structure with 5 nm thick Al_2O_3 film. It was found in Ref [25] that the layer AlO_x in the $ITO/AlO_x/HfO_2/AlO_x/TiN$ structure already at a thickness of 0.5 nm performs the function of a diffusion barrier at both the lower and upper interface and stabilizes the current carrying capacity of the filament, which leads to low switching voltages and significantly increases the RS quantity. It is noted that AlO_x influence changed with an increase of thickness of its layer from 2 to 5 nm— in addition to the role of the tunnel barrier, it began to take an active part in RS, which manifested itself in an increase in the spread of RS parameters. It was found in Ref. [26] that the presence of an additional 3 nm thick layer of Al_2O_3 at the interface with the lower and/or upper electrode in memristor structures of $Pt/Al_2O_3/HfO_2/Al_2O_3/Ti$ leads to an increase of R_{HRS}/R_{LRS} ratio by almost an order of magnitude, which allows for multi-level switching in such structures.

There is no unified understanding in the literature about the causes of such an influence despite a significant number of results demonstrating the effect of additional insulating layers and their thickness on the parameters of RS memristor structures. As a rule, the authors agree that a single filament of oxygen vacancies is formed in different layers of the multilayer structure, but its fragments located in these layers are destroyed and restored in different ways during the RS process. Moreover, there are opposing opinions on this matter. In particular, it is assumed that in two-layer and multilayer structures of Al_2O_3/HfO_2 the restoration and destruction of the filament in the RS process occurs in the layer Al_2O_3 [18,24], since the electric field in Al_2O_3 is about 3 times greater than in HfO_2 due to the difference of the permittivity of the layers [26]. At the same time, other papers claim that the destruction of the filament occurs at the boundary of the Al_2O_3 layer with a functional dielectric layer (TiO_x [11], TaO_x [16] or HfO_x [22]), while the part of the filament formed in the Al_2O_3 layer is preserved during cyclic switching due to the limited diffusion of oxygen vacancies in Al_2O_3 [27]. It should be noted that the characteristics of memristor structures based on two-layer (multilayer) oxide dielectrics depend not only on the combination of dielectric layers, but also on the choice of electrode material [28] and the technology of manufacturing of memristor structures [29,30].

This paper presents the results of an experimental study of the effect of an additional insulating layer Al_2O_3 and its thickness (0, 3, 6 and 9 nm) on the parameters of resistive switching of memristors based on a two-layer dielectric $Al_2O_3/ZrO_2(Y)$ obtained by magnetron deposition.

The choice of yttrium-stabilized zirconium dioxide ($ZrO_2(Y)$) as a functional layer of the memristor structure is associated with favorable conditions for the implementation of RS in this material: high mobility of oxygen ions [31], as well as the ability to control the concentration of oxygen vacancies by changing the amount of a stabilizing additive Y_2O_3. The energy of formation of an active (mobile) oxygen vacancy in ZrO_2 (12.5 mol.% Y_2O_3) can have a relatively small value of 0.6 eV [32]. The high mobility of oxygen ions in $ZrO_2(Y)$ compared with other oxides is also associated with a relatively low activation energy of oxygen ion migration through oxygen vacancies $E_a = 0.58-0.65$ eV [33,34]. The possibility of effective use of memristors based on $ZrO_2(Y)$ for the creation of neuromorphic electronics devices is demonstrated in Ref. [35], therefore, it is a promising material for creating memristor devices.

1. Materials and methods

The paper studied the structures of Pt(20 nm)/Ta(40 nm)/ Al_2O_3(0, 3, 6, 9 nm)/$ZrO_2(Y)$(20 nm)/Pt(40 nm)/Ti(10 nm) formed by magnetron deposition on oxidized silicon substrates of SiO_2/Si metallized with TiN/Ti layers. The Torr International 2G1-1G2-EB4-TH1 thin film deposition vacuum system was used to form multilayer memristor structures.

$ZrO_2(Y)$ and Al_2O_3 films were applied by high-frequency magnetron sputtering at substrate temperature of 250°C. A target compressed from a mixture of powders ZrO_2 (88 mol.%) and Y_2O_3 (12 mol.%) was used for application of $ZrO_2(Y)$ films. The bottom electrodes (Pt) with an adhesive layer (Ti), as well as the top electrodes (Ta) with a protective layer (Pt) were applied by direct current magnetron sputtering at a temperature of 200°C.

The upper electrodes with a protective layer were formed through a shadow mask with holes for electrical measurements. The area of the upper electrodes was $S \approx 1.3 \cdot 10^{-3}\,cm^2$. Structures with continuous layers of the upper electrode and the protective layer were made for studies using X-ray photoelectron spectroscopy (XPS).

The electrical characteristics of the structures were measured using the Agilent B1500A semiconductor device parameter analyzer using the EverBeing EB-6 analytical probe station. The voltage sign on the structures corresponded to the potential of the upper electrode (Ta) relative to

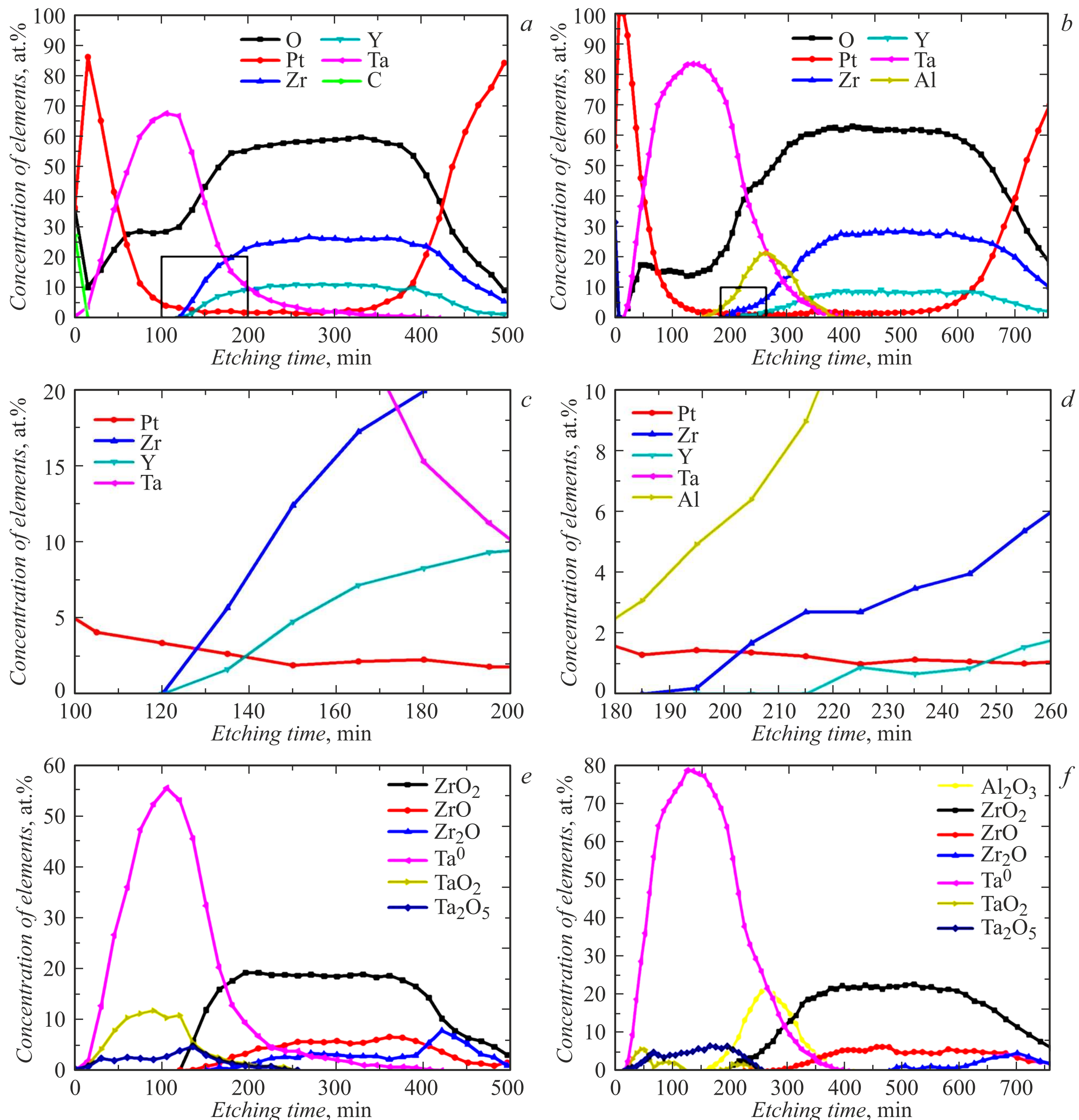

Figure 1. Concentration distribution profiles of elements (*a–d*) and chemical compounds (*e,f*) depending on the etching time of the structures $Ta/ZrO_2(Y)/Pt$ (*a, c, e*) and Ta/Al_2O_3 (6 nm)/$ZrO_2(Y)/Pt$ (*b, d, f*), measured during the layered analysis by the XPS method.

the potential of the lower electrode (Pt). The current limitation (I_{CC}) was implemented using the Agilent B1500A software for measuring the current-voltage curve.

The phase analysis of memristor structures was carried out by the XPS method using the Multiprobe RM system (Omicron Nanotechnology GmbH, Germany). The depth profiling was carried out by etching with Ar^+ ions at an energy of 1 keV. The maximum detectable concentration of elements is 0.5,at.%. The error of determination of the depth did not exceed 2–3 nm. See [36] for a more detailed description of the technique. Photoelectronic lines were recorded to determine the concentration of chemical elements: O 1s, C 1s, Zr 3d, Y 3d, Pt 4f, Al 2s. The spectra were analyzed using data on chemical shifts and positions of photoelectron lines [37,38].

2. Results and discussion

Fig. 1 shows the results of an XPS study of the elemental and chemical composition of the structures of

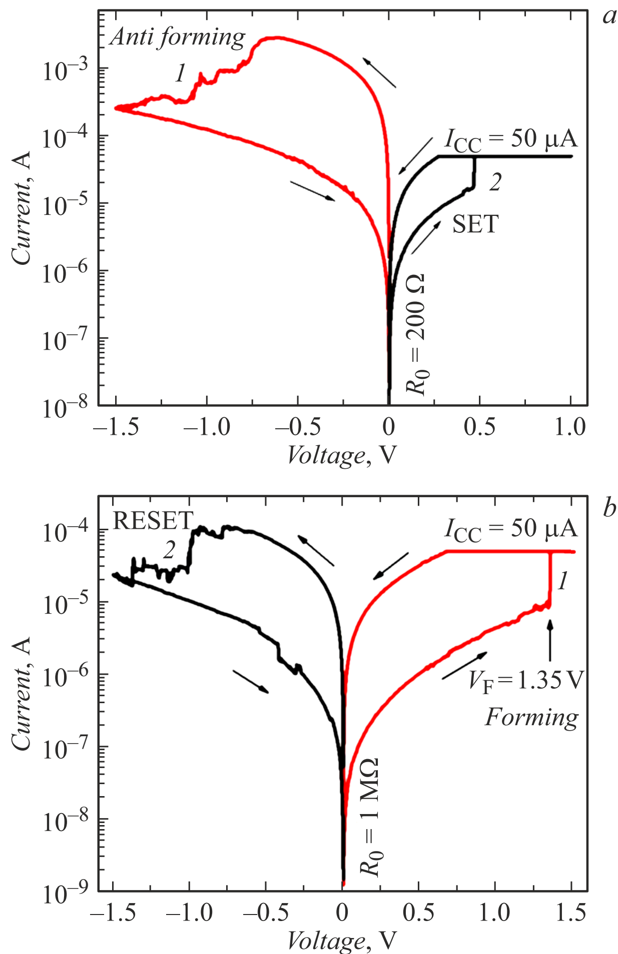

Figure 2. Current-voltage curves, demonstrating the process of „antiforming" of the initially conductive structure of $Ta/ZrO_2(Y)/Pt$ and the subsequent SET process (*a*), and the process of electroforming of the initially non-conductive structure of Ta/Al_2O_3 (6 nm)$/ZrO_2(Y)/Pt$ and the subsequent RESET process (*b*). The initial resistance of the structures (R_0) was 200 Ω and 1 MΩ, respectively.

$Ta/ZrO_2(Y)/Pt$ and Ta/Al_2O_3(6 nm)$/ZrO_2(Y)/Pt$ immediately after formation. It can be seen that the upper electrode (Ta) of both structures is oxidized, as evidenced by the distribution profile of the concentration of oxygen atoms (Fig. 1, *a, b*). Moreover, the number of oxygen atoms in the Ta electrode in the structure containing the Al_2O_3 layer is almost 3 times less, and in there is an inflection of the profile distribution of the concentration of oxygen atoms in the area of localization of the Al_2O_3 layer (Fig. 1, *b*), which indicates a restriction of oxygen diffusion into Ta electrode from $ZrO_2(Y)$ by Al_2O_3 layer.

A more detailed analysis of the distribution of chemical elements on the heterogeneous boundary of the dielectric layer with Ta (marked with black rectangles in Fig. 1, *a, b*) is shown in Fig. 1, *c, d*. It can be seen that the detection of Zr and Y begins at the site of signal growth from Al at the $Ta/Al_2O_3/ZrO_2(Y)$ heteroboundary, in addition, there is a feature in the Zr concentration distribution profile (step) (fig. 1, *d*). The occurrence of a signal from $ZrO_2(Y)$ after etching part of Al_2O_3 layer indicates the heterogeneity of the layers in thickness, and the absence of signal growth from Zr during the etching time from 215 to 225 min suggests that ZrO_2 is concentrated in the aluminum oxide layer in local areas, the area of which does not increase (or slightly increases) during ion etching. After passing the step, the concentrations of the elements Zr and Y monotonously increase (Fig. 1, *d*), as well as in the structure without Al_2O_3 (Fig. 1, *c*).

Grain boundaries may be local areas in which $ZrO_2(Y)$ is concentrated in the Al_2O_3. It was shown earlier using high-resolution transmission electron microscopy in Ref. [39] that $ZrO_2(Y)$ layers deposited by magnetron sputtering have a columnar polycrystalline structure and a developed upper boundary with irregularities of the order 1–5 nm, corresponding to the positions of the grain boundaries in the $ZrO_2(Y)$ film.

The chemical analysis results shown in Fig. 1, *e, f* demonstrate the presence of elementary Ta^0 and compounds of TaO_2 and Ta_2O_5 in the Ta layer. A similar result was obtained in Ref. [40–42], where it was shown that the oxidation of the active ohmic electrode occurs from the side of the oxide dielectric. Asignificantly higher amount of TaO_2 is observed in a structure that does not contain Al_2O_3 (Fig. 1, *e*). This indicates partial oxidation of the

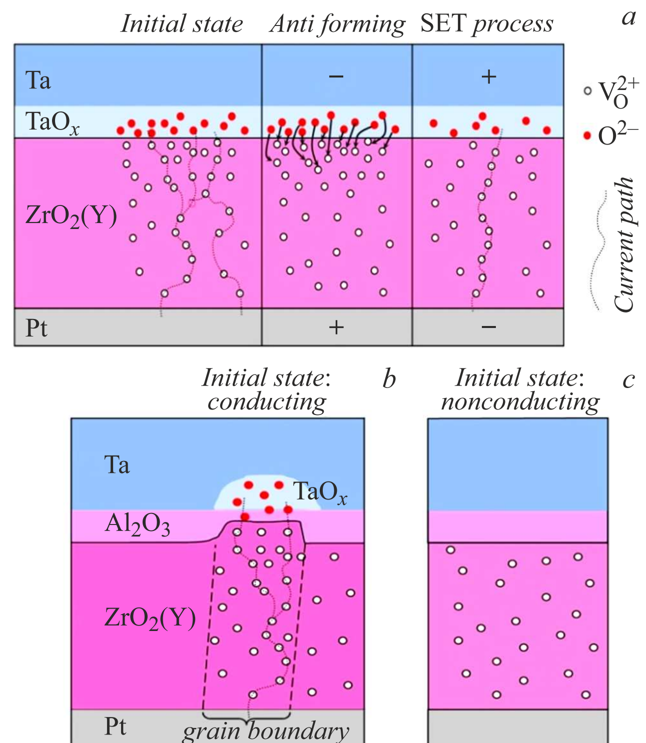

Figure 3. Schematic representation of the initial conductive state, antiforming and SET process for structures of $Ta/ZrO_2(Y)/Pt$ (*a*) and two initial states of two-layer structures of $Ta/Al_2O_3/ZrO_2(Y)/Pt$ (*b, c*).

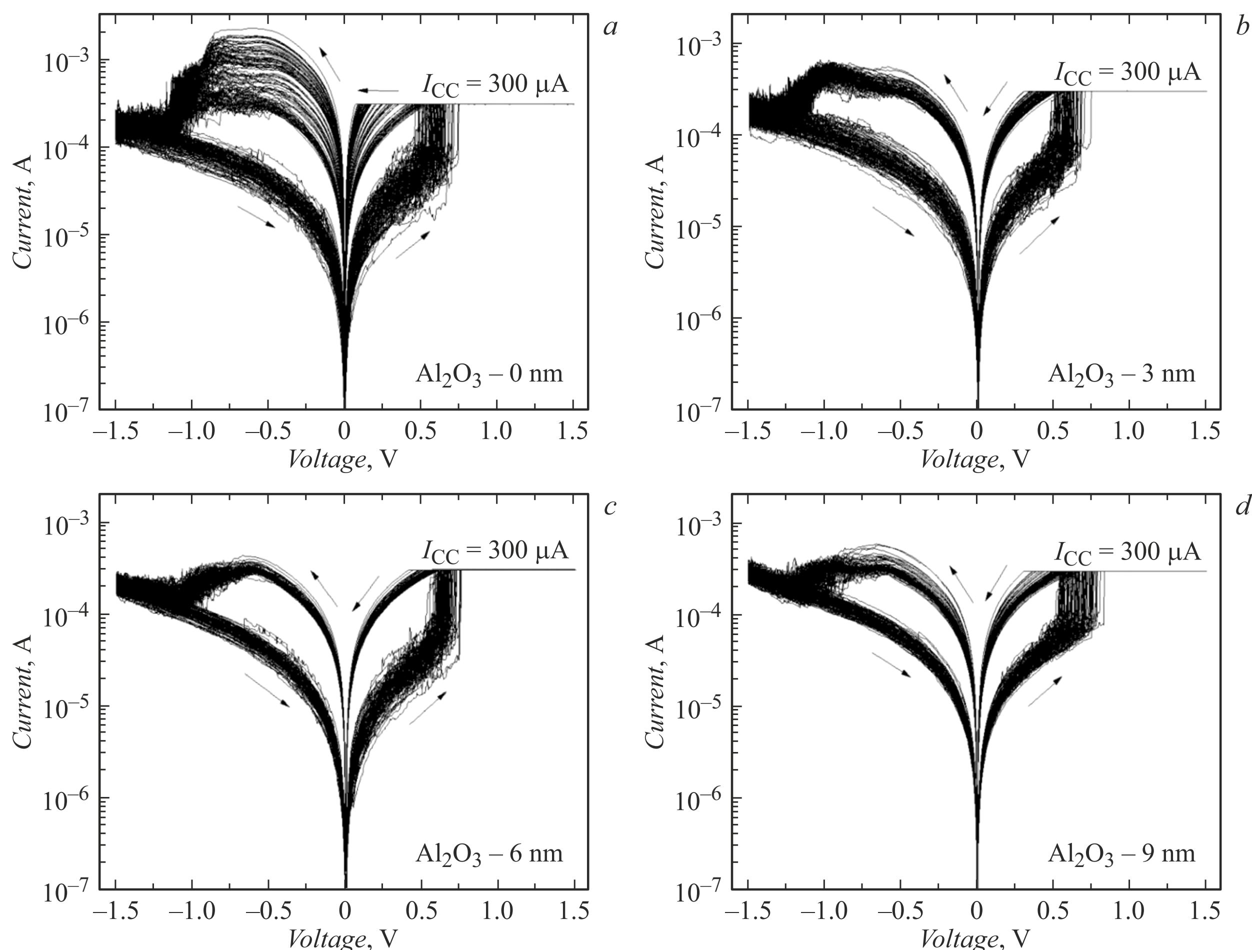

Figure 4. Typical series of 100 current-voltage curves of $Ta/Al_2O_3/ZrO_2(Y)/Pt$ structures with different thickness of additional insulating layer of Al_2O_3 — 0 (it a), 3 (it b), 6 (it c) and 9 nm (*d*).

upper electrode due to the diffusion of oxygen atoms from the $ZrO_2(Y)$ layer during the formation of the memristor structure, as well as the fact that the additional Al_2O_3 layer blocks such diffusion.

It should be noted that the initial resistance of oxide memristor structures is determined by the initial concentration of oxygen vacancies in the resistive layer, which depends on many conditions, including the manufacturing method. In particular, structures based on Al_2O_3/HfO_2 obtained by atomic layer deposition [24,25,43] were initially in a non-conductive state and required preliminary electroforming even with small thicknesses of resistive layers (2−6 nm). Whereas the two-layer structure of AlO_x (3 nm)/TaO_x (5 nm) [44] grown by electron beam evaporation demonstrated initial resistance $\sim 200\,\Omega$ and required the initial process of „antiforming" at voltages slightly higher than V_{RESET} during subsequent cyclic measurements of the current-voltage curve.

The results of measurement of electrical characteristics in this paper showed that all memristor structures with an additional insulating layer of Al_2O_3 with thickness equal to 0 and 3 nm, were initially in a conductive state. Fig. 2, *a* shows typical curves of the first cycle of the current-voltage curves of $Ta/ZrO_2(Y)/Pt$ structures, for which antiforming was performed prior to RS (by applying negative voltage).

The results obtained can be interpreted as follows (Fig. 3, *a*). It is assumed that the diffusion of oxygen from $ZrO_2(Y)$ into the Ta electrode and its partial oxidation during deposition contribute to an increase of the concentration of oxygen vacancies in the $ZrO_2(Y)$ layer to values sufficient for the formation of conductive channels in the initial memristor structures (Initial state in Fig. 3, a), which leads to the fact that initially the structures demonstrate a conductive state (the initial resistance is 50−700 Ω). Al_2O_3 layer with a thickness of 3 nm is presumably diffusionally transparent and does not interfere with the oxidation of the electrode Ta. The application of negative voltage to the Ta electrode during antiforming leads to the drift of oxygen ions from the TaO_x layer into the $ZrO_2(Y)$ layer, where they recombine with oxygen vacancies, increasing the resistance of the memristor structure and converting it to HRS. The process of filament formation begins when the positive voltage is subsequently applied to the Ta electrode

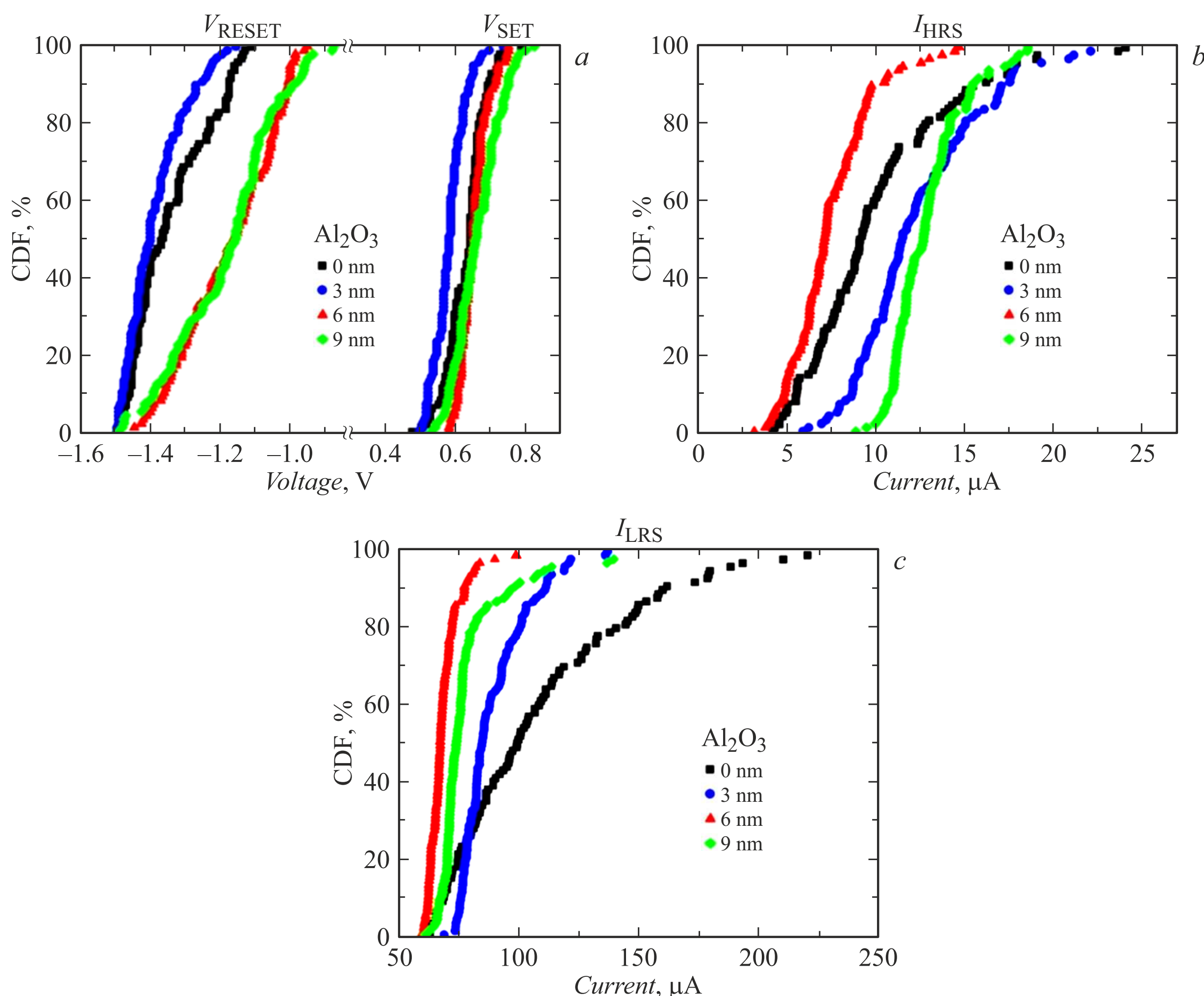

Figure 5. Cumulative distribution functions (CDF) of switching voltages V_{SET} and V_{RESET} (*a*) and current states of the memristor (at reading voltage $V_{read} = 0.15$ V) I_{HRS} (*b*) and I_{LRS} (*c*) from cycle to cycle according to the current-voltage curve data shown in Fig. 4.

in the result of which the structure enters into a LRS (the SET process in Fig. 3, *a*).

About 50% of the studied memristors in 6 and 9 nm thick structures with Al_2O_3 were initially in a non-conductive state and required electroforming by applying a positive voltage (Fig. 2, *b*). The average value of the electroforming voltage (V_F) in structures with Al_2O_3 with a thickness of 6 nm was +1.67 V, and it was +2.33 V in structures with a thickness of 9 nm. This is consistent with the literature data according to which the electroforming voltage of memristor devices varies directly proportional to the thickness of the dielectric and inversely proportional to the square root of the permittivity [45].

It is assumed that the initial conducting state in two-layer memristor structures with 6 and 9 nm thick Al_2O_3 is attributable to local areas of inhomogeneity of Al_2O_3 film and the grain boundaries of $ZrO_2(Y)$ polycrystalline film (Fig. 3, *b*), which is confirmed by the XPS data. The highest diffusion transparency and mobility of oxygen ions are realized and the formation of conducting channels is most likely in the area of these particular structural defects [38,46,47]. Fig. 3, *b* shows that the Ta electrode is oxidized, simultaneously increasing the concentration of vacancies in the $ZrO_2(Y)$ layer in this case at the area of local thinning of Al_2O_3 films like in case of the absence of an additional barrier layer. The difference from the structure without the Al_2O_3 layer is that not the entire electrode area is oxidized (Fig. 3, *a*), but the local area near the grain boundaries of the $ZrO_2(Y)$ film (fig. 3, *b*). In this case, $Ta/Al_2O_3/ZrO_2(Y)/Pt$ structure initially also appears in a conductive state. At the same time, the initial resistance of the conductive structures increases with an increase of the thickness of Al_2O_3 layer: $\sim 700\,\Omega$ for 3 nm thick film, $\sim 1.5\,k\Omega$ — for 6 nm thick film and $\sim 4.2\,k\Omega$ — for 9 nm thick film. It is necessary to perform the „antiforming" process to implement RS in such memristors.

If Al_2O_3 film under Ta electrode turns out to be heterogeneous and diffusionally opaque in case of application of Ta electrode, (Fig. 3, *c*), then it blocks the diffusion of oxygen into the active metal electrode, which does not

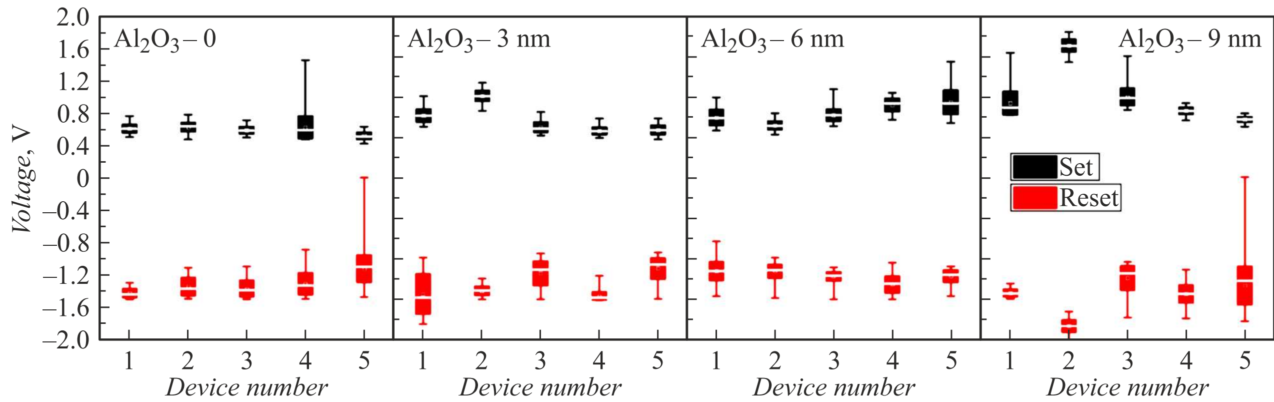

Figure 6. Dependence of the switching voltage variability V_{SET} and V_{RESET} from device to device for Ta/Al_2O_3/ZrO_2(Y)/Pt structure with different thickness of Al_2O_3 layer.

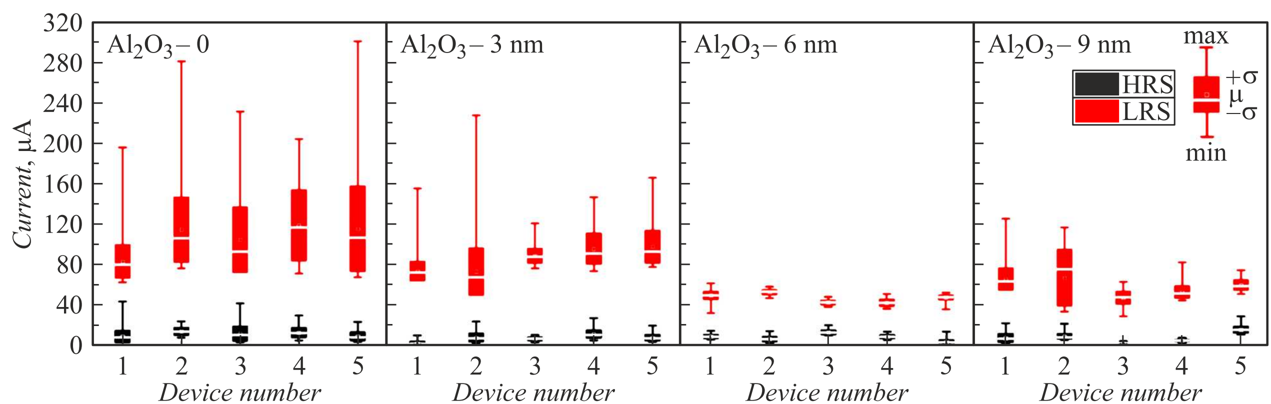

Figure 7. Dependence of current variability (at reading voltage $V_{Read} = 0.15\,V$) I_{HRS} and I_{LRS} from device to device for Ta/Al_2O_3/ZrO_2(Y)/Pt structures with different thickness of Al_2O_3 layer.

lead to a significant change of the vacancy concentration in the functional dielectric layer of ZrO_2(Y). Such structures are initially in a non-conductive state and require electroforming.

An interesting feature should be noted — both types of structures, which were initially in conductive or non-conductive states and underwent antiforming and electroforming procedures, respectively, after several cycles of current-voltage curve measurement, did not demonstrate significant differences of the values of currents in LRS and HRS and switching voltages V_{SET} and V_{RESET}.

The results of measurement of current-voltage curves of Ta/Al_2O_3/ ZrO_2(Y)/Pt structures with different thickness of the additional insulating layer of Al_2O_3 are shown in fig. 4. The switching voltages did not exceed the values of $\pm 1.5-2\,V$ for all studied structures. Figure 5 shows the results of statistical processing of the current-voltage curve series in Figure 4. It can be seen that the switching voltages V_{SET} and their spread practically do not change in case of addition of Al_2O_3, the voltage spread V_{RESET} slightly increases with an increase of the thickness (in the case of 6 and 9 nm thick Al_2O_3) (Fig. 5, *a*). At the same time, the presence of the Al_2O_3 layer significantly reduces the spread of current values (Fig. 5, *b, c*), especially in LRS.

The variability of the resistive switching parameters from device to device is shown in Fig. 6 and 7. It can be seen that the switching voltages V_{SET} and V_{RESET} slightly change with the addition of an additional insulating layer of Al_2O_3. It is necessary to note a significantly smaller spread of current states in the structure of Ta/Al_2O_3 (6 nm)/ZrO_2(Y)/Pt, despite the smallest current corridor (Fig. 7).

5 structures Ta/ZrO_2(Y)/Pt and Ta/Al_2O_3 (6 nm)/ ZrO_2(Y)/Pt were tested for resistance to multiple RS. All of them withstood over $1 \cdot 10^6$ RP cycles in pulse mode, maintaining voltages of switching to high-resistance and low-resistance states and current corridors.

The improvement of current stability in the LRS does not depend on the initial resistive state of the memristor structure. It is assumed that in the case of local heterogeneity of the Al_2O_3 layer (Fig. 3, *b*), part of the filament can be localized in places of such heterogeneity, which is associated with limited lateral diffusion mobility of oxygen ions (oxygen vacancies) in aluminum oxide. This helps to preserve the area of destruction and subsequent

restoration of the filament during cyclic switching. In the case of a homogeneous layer of Al_2O_3 (Fig. 3, *c*) initially formed during electroforming in a two-layer structure of $Al_2O_3/ZrO_2(Y)$ part of the filament in the Al_2O_3 layer may also be preserved due to limited diffusion of oxygen vacancies in Al_2O_3. This is attributable to the high values of the energy of formation of oxygen vacancies in Al_2O_3 (6−8 eV [27,31]) and the activation energy of oxygen ion migration along oxygen vacancies (1.3–1.7 eV [28.31]) compared to the corresponding values for ZrO_2(Y).

Conclusion

An experimental study of the effect of an additional dielectric layer of Al_2O_3 and its thickness (0, 3, 6 and 9 nm) on the parameters of resistive switching of memristor structures of $Ta/Al_2O_3/ZrO_2(Y)/Pt$.

It was found that memristor structures made by magnetron sputtering without a layer of Al_2O_3, as well as with its small thickness (3 nm), are initially in a conductive state and require antiforming at voltages for the onset of resistive switching, practically not different from the voltages V_{RESET} during subsequent resistive switching.

Structures with an additional 6 and 9 nm thick dielectric layer of Al_2O_3 can initially be in both conductive and non-conductive states. It was found that both types of structures, initially in different resistive states and having undergone antiforming and electroforming procedures, after several cycles of current-voltage curve measurement did not demonstrate significant differences of the values of currents and switching voltages during subsequent measurements.

The results of the study showed that the use of an additional layer of Al_2O_3 improves the stability of current states, which is most pronounced in case of 6 nm thickness of Al_2O_3 layer. At the same time, the presence of an additional layer of Al_2O_3 does not have a significant effect on the values of switching voltages and their spread.

Pulse measurements demonstrate more than 10^6 of resistive switching, which makes it possible to use structures based on a two-layer dielectric $Al_2O_3/ZrO_2(Y)$ as elements of non-volatile resistive memory.

The results obtained can be used to fabricate „non-forming“ memristor structures, which is important for CMOS integration of such devices.

Funding

The study was performed under the State Assignment No FSWR-2022-0009. The study was conducted using the equipment of the Center for Collective Use of the Scientific and Educational Center „Physics of Solid-State Nanostructures“ and the Educational Design Center of Electronics of Lobachevsky State University of Nizhny Novgorod.

Conflict of interest

The authors declare that they have no conflict of interest.

References

[1] D. Zhu, Y. Li, W. Shen, Z. Zhou, L. Liu, X. Zhang. J. Semicond., **38** (7), 071002 (2017). DOI: 10.1088/1674-4926/38/7/071002

[2] A.N. Mikhailov, E.G. Gryaznov, V.I. Lukoyanov, M.N. Koryazhkina, I.A. Bordanov, S.A. Shchanikov, O.A. Telminov, M.V. Ivanchenko, V.B. Kazantsev. Fizmat, **1** (1), 42 (2023) (in Russian). DOI: 10.56304/S2949609823010021

[3] F. Zahoor, T.Z.A. Zulkifli, F.A. Khanday. Nanoscale Res. Lett., **15** (1), 90 (2020). DOI: 10.1186/s11671-020-03299-9

[4] J.S. Lee, S. Lee, T.W. Noh. Appl. Phys. Rev., **2** (3), 031303 (2015). DOI: 10.1063/1.4929512

[5] D.S. Jeong, R. Thomas, R.S. Katiyar, J.F. Scott, H. Kohlstedt, A. Petraru, C.S. Hwang. Rep. Prog. Phys., **75** (7), 076502 (2012). DOI: 10.1088/0034-4885/75/7/076502

[6] X.-D. Huang, Y. Li, H.-Y. Li, K.-H. Xue, X. Wang, X.-S. Miao. IEEE Electron Device Lett., **41** (4), 549 (2020). DOI: 10.1109/LED.2020.2977397

[7] T.-L. Tsai, Y.-H. Lin, T.-Y. Tseng. IEEE Electron Device Lett., **36** (7), 675 (2015). DOI: 10.1109/LED.2015.2428719

[8] D. Ielmini. Semicond. Sci. Technol., **31** (6), 063002 (2016). DOI: 10.1088/0268-1242/31/6/063002

[9] H. Wu, X. Li, M. Wu, F. Huang, Z. Yu, H. Qian. IEEE Electron Device Lett., **35** (1), 39 (2014). DOI: 101109/LED.2013.2288311

[10] M. Trapatseli, S. Cortese, A. Serb, A. Khiat, T. Prodromakis. J. Appl. Phys., **121** (18), 184505 (2017). DOI: 10.1063/1.4983006

[11] L. Alekseeva, T. Nabatame, T. Chikyow, A. Petrov. Jpn. J. Appl. Phys., **55** (8S2), 08PB02 (2016). DOI: 10.7567/JJAP.55.08PB02

[12] U. Chand, C.-Y. Huang, T.-Y. Tseng. IEEE Electron Device Lett., **35** (10), 1019 (2014). DOI: 10.1109/LED.2014.2345782

[13] M. Ismail, H. Abbas, C. Choi, S. Kim. J. Alloys Compd., **835**, 155256 (2020). DOI: 10.1016/j.jallcom.2020.155256

[14] O.N. Gorshkov, I.N. Antonov, A.I. Belov, A.P. Kasatkin, A.N. Mikhailov. Pis'ma v ZhTF,**40** (3), 12 (2014) (in Russian).

[15] L. Jiang, Y. Jin, Y. Zhao, J. Meng, J. Zhang, X. Chen, X. Wu, Y. Xiao, Z. Tao, B. Jiang, X. Wen, C. Ye. Adv. Phys. Res., **2** (5), 2200086 (2023). DOI: 10.1002/apxr.202200086

[16] X.A. Tran, H.Y. Yu, B. Gao, J.F. Kang, X.W. Sun, Y.-C. Yeo, B.Y. Nguyen, M.F. Li. IEEE Electron Dev. Lett., **32** (9), 1290 (2011). DOI: 10.1109/LED.2011.2161259

[17] C.-Y. Huang, J.-H. Jieng, W.-Y. Jang, C.-H. Lin, T.-Y. Tseng. ECS Solid State Lett., **2** (8), 63 (2013). DOI: 10.1149/2.006308ssl

[18] Z. Chen, F. Zhang, B. Chen, Y. Zheng, B. Gao, L. Liu, X. Liu, J. Kang. Nanoscale Res. Lett., **10** (1), 70 (2015). DOI: 10.1186/s11671-015-0738-1

[19] R. Han, P. Huang, Y. Zhao, Z. Chen, L. Liu, X. Liu, J. Kang. Nanoscale Res. Lett., **12** (1), 37 (2017). DOI: 10.1186/s11671-016-1807-9

[20] J. Woo, K. Moon, J. Song, S. Lee, M. Kwak, J. Park, H. Hwang. IEEE Electron Dev. Lett., **37** (8), 994 (2016). DOI: 10.1109/LED.2016.2582859

[21] M. Akbari, M.-K. Kim, D. Kima, J.-S. Lee. RSC Adv., **7** (27), 16704 (2017). DOI: 10.1039/C6RA26872B

[22] M.K. Mahadevaiah, E. Perez, M. Lisker, M.A. Schubert, E.P.B. Quesada, C. Wenger, A. Mai. Electronics, **11** (10), 1540 (2022). DOI: 10.3390/electronics11101540

[23] L. Chen, Y.-W. Dai, Q.-Q. Sun, J.-J. Guo, P. Zhou, D.W. Zhang. Solid State Ionics, **273**, 66 (2015). DOI: 10.1016/j.ssi.2014.08.014

[24] K.-M. Persson, M.S. Ram, L.-E. Wernersson. IEEE J. Electron Dev. Society, **9**, 564 (2021). DOI: 10.1109/JEDS.2021.3079398

[25] J. Liu, H. Yang, Z. Ma, K. Chen, X. Zhang, X. Huang, S. Oda. J. Phys. D: Appl. Phys., **51** (2), 025102 (2017). DOI: 10.1088/1361-6463/aa9c15

[26] J. Robertson. The Europ. Phys. J. Appl. Phys., **28** (3), 265 (2004). DOI: 10.1051/epjap:2004206

[27] *Resistive Switching: From Fundamentals of Nanoionic Redox Processes to Memristive Device Applications*. Ed. by D. Ielmini, R. Waser (Wiley-VCH Verlag GmbH & Co. KGaA, Germany, 2016)

[28] Y. Guo, J. Robertson. Appl. Phys. Lett., **105** (22), 223516 (2014). DOI: 10.1063/1.4903470

[29] M. Gerasimova, A. Ivanov, D. Mazing, D. Chigirev, N. Andreeva. J. Phys.: Conf. Ser., **1697** (1), 012129 (2020). DOI: 10.1088/1742-6596/1697/1/012129

[30] A.N. Mikhaylov, M.N. Koryazhkina, D.S. Korolev, A.I. Belov, E.V. Okulich, V.I. Okulich, I.N. Antonov, R.A. Shuisky, D.V. Guseinov, K.V. Sidorenko, M.E. Shenina, E.G. Gryaznov, S.V. Tikhov, D.O. Filatov, D.A. Pavlov, D.I. Tetelbaum, O.N. Gorshkov, A.V. Emelyanov, K.E. Nikiruy, V.V. Rylkov, V.A. Demin, B. Spagnolo. In: *Metal Oxides for Non-volatile Memory* ed. by P. Dimitrakis, I. Valov, S. Tappertzhofen (Elsevier, 2022)

[31] H.A. Abbas. *Stabilized Zirconia for Solid Oxide Fuel Cells or Oxygen Sensors: Characterization of Structural and Electrical Properties of Zirconia Doped with Some Oxides* (LAP Lambert Academic, 2012)

[32] V.G. Zavodinsky. FTT, **46** (3), 441 (2004) (in Russian).

[33] S. Tikhov, O. Gorshkov, I. Antonov, A. Morozov, M. Koryazhkina, D. Filatov. Adv. Conden. Matter. Phys., **2018** (8), 2028491 (2018). DOI: 10.1155/2018/2028491

[34] A.V. Yakimov, D.O. Filatov, O.N. Gorshkov, D.A. Antonov, D.A. Liskin, I.N. Antonov, A.V. Belyakov, A.V. Klyuev, A. Carollo, B. Spagnolo. Appl. Phys. Lett., **114** (25), 253506 (2019). DOI: 10.1063/1.5098066

[35] A.V. Emelyanov, K.E. Nikiruy, V.A. Demin, V.V. Rylkov, A.I. Belov, D.S. Korolev, E.G. Gryaznov, D.A. Pavlov, O.N. Gorshkov, A.N. Mikhaylov, P. Dimitrakis. Microelectron. Engineer., **215**, 110988 (2019). DOI: 10.1016/j.mee.2019.110988

[36] S.Yu. Zubkov, I.N. Antonov, O.N. Gorshkov, A.P. Kasatkin, R.N. Kryukov, D.E. Nikolichev, D.A. Pavlov, M.E. Shenina. FTT, **60** (3), 591 (2018) (in Russian). DOI: 10.21883/FTT.2018.03.45566.249

[37] F. Iacona, R. Kelly, G. Marletta. J. Vac. Sci. Technol. A, **17** (5), 2771 (1999). DOI: 10.1116/1.581943

[38] M.-S. Kim, Y.-D. Ko, J.-H. Hong, M.-C. Jeong, J.-M. Myoung, I. Yun. Appl. Surf. Sci., **227** (1–4), 387 (2004). DOI: 10.1016/j.apsusc.2003.12.017

[39] O.N. Gorshkov, A.N. Mikhaylov, A.P. Kasatkin, S.V. Tikhov, D.O. Filatov, D.A. Pavlov, A.I. Belov, M.N. Koryazhkina, A.I. Bobrov, N.V. Malekhonova, E.G. Gryaznov, I.N. Antonov, M.E. Shenina. J. Phys.: Conf. Ser., **741** (1), 012174 (2016). DOI: 10.1088/1742-6596/741/1/012174

[40] A. Kindsmüller, A. Meledin, J. Mayer, R. Waser, D. Wouters. Nanoscale, **11** (39), 18201 (2019). DOI: 10.1039/c9nr06624a

[41] C.-Y. Lin, C. Wu, C.-Y. Wu, T.-C. Lee, F.-L. Yang, C. Hu, T. Tseng. IEEE Electron Dev. Lett., **28** (5), 366 (2007). DOI: 10.1109/LED.2007.894652

[42] S. Chen, I. Valov. Adv. Mater., **34** (3), 2105022 (2022). DOI: 10.1002/adma.202105022

[43] J. Liu, H. Yang, Z. Ma, K. Chen, X. Zhang, X. Huang, S. Oda. J. Phys. D: Appl. Phys., **51** (2), 025102 (2017). DOI: 10.1088/1361-6463/aa9c15

[44] S. Liu, Y. Sun, B. Song, Z. Li, H. Liu, Q. Li. Phys. Lett. A, **383** (30), 125877 (2019). DOI: 10.1016/j.physleta.2019.125877

[45] J.W. McPherson, J. Kim, A. Shanware, H. Mogul, J. Rodriguez. IEEE Transactions on Electron Dev., **50** (8), 1771 (2003). DOI: 10.1109/TED.2003.815141

[46] M. Lanza, K. Zhang, M. Porti, M. Nafría, Z.Y. Shen, L.F. Liu, J.F. Kang, D. Gilmer, G. Bersuker. Appl. Phys. Lett., **100** (12), 123508 (2012). DOI: 10.1063/1.3697648

[47] M. Lanza, G. Bersuker, M. Porti, E. Miranda, M. Nafría, X. Aymerich. Appl. Phys. Lett., **101** (19), 193502 (2012). DOI: 10.1063/1.4765342

Translated by A.Akhtyamov